Experimental setup to characterize flow-induced anisotropy of sheet metals

IOP Conf. Series: Materials Science and Engineering **418** (2018) 012085 doi:10.1088/1757-899X/418/1/012085

Experimental setup to characterize flow-induced anisotropy of sheet metals

F Gutknecht[*1], G Gerstein[2], H Traphöner[1], T Clausmeyer[1] and F Nürnberger[2]

[1] Institute of Forming Technology and Lightweight Components (IUL), TU Dortmund University, Baroper Str. 303, 44227 Dortmund, Germany
[2] Institut für Werkstoffkunde (Materials Science), Leibniz Universität Hannover, An der Universität 2, Garbsen, Germany

E-Mail: Florian.Gutknecht@iul.tu-dortmund.de

Abstract. For many metals, a transient variation of the yield stress can be observed when changing the orientation of a load-path. Such behavior affects the manufacturing process itself, e.g. by increasing forming forces, altered material properties or springback of the manufactured components. Hence, the aim of this work is to develop a novel experimental setup to characterize hardening effects due to flow-induced anisotropy for sheet metals. The proposed experiment consists of two subsequent forming operations. Initially, a hydraulic bulge test is conducted, followed by torsion of the hemispherical preformed sheet. Such approach captures the effects of flow-induced anisotropy like cross hardening as could be proved for the example of the conventional deep-drawing steel DC04. The benefits of the presented setup are (i) high plastic strains in the pre-loading step and (ii) determination of several combinations of pre- and subsequent loading.

1. Introduction

Early reference for flow-induced anisotropy is given by Bauschinger in the 19th century [1]. Since then the effect of decreased yield stress after load-reversal has become well-known as the Bauschinger effect. Many sheet forming applications benefit from the knowledge of this phenomenon connected to the microstructural evolution and a quantitative description enabled by numerical simulation. With the increasing complexity of the forming path in modern processes (e.g. sheet-bulk metal forming) attention should be paid to more general load path changes [2]. Ghosh and Backofen [3] observed an increased initial yield stress after reloading in orthogonal direction. This effect is called cross-hardening and has been reported repeatedly for low alloyed single-phase steels.

Usually, the effect of cross-hardening is followed by a transient hardening stagnation, or even softening. The length of this transition has been found to be related to the prestrain by Rauch and Schmitt [4]. Additionally, they have linked the observed phenomena to the evolution of dislocation walls in the microstructure. The increase of the yield stress is due to activation of latent glide systems. With increasing deformation, microbands are developing and destabilize the created dislocation walls. Therefore low-alloyed single-phase steels are expected to be sensitive, while high alloyed multi-phase steels have reduced mobility of dislocations.

The normalized scalar product κ of prestrain $\boldsymbol{D}(t_n)$ and subsequent strain $\boldsymbol{D}(t_{n+1})$ has been proposed by Schmitt et al. [5] to quantify the change in strain path. Here κ represents the cosine of the angle

between the two strain directions in the plane of deformation. For monotonic deformation $\kappa = 1$, load reversal yields $\kappa = -1$, and an orthogonal strain path change is obtained with $\kappa = 0$.

$$\kappa = \frac{\boldsymbol{D}(t_n)}{|\boldsymbol{D}(t_n)|} \cdot \frac{\boldsymbol{D}(t_{n+1})}{|\boldsymbol{D}(t_{n+1})|} \tag{1.1}$$

Since the early observations researchers have used different setups to investigate and characterize the effects active for $\kappa = 0$. Early setups employed uniaxial tensile tests with various starting and subsequent loading directions (e.g. [6], [7]). Though these tests only allow small prestrains and subsequent specimens have to be manufactured by destruction of the previous. Later setups with plane-strain condition at prestrain have been proposed (e.g. [8], [9]). Those specimen can be tested without manipulation between the loading steps. It has been found that the effect of cross-hardening is strongest for sharp changes and lowest for smooth transitions. Yet plane-strain tension only allows small strains. Other researchers have used combination of shear test at different angle to obtain high prestrain ([10]), though these also require the destruction of the previous specimen. Moreover, it is difficult to obtain an ideal shear state in tensile testing devices.

2. Methods

2.1. Experimental setup

2.1.1. General considerations. The proposed experiment includes two steps (Figure 1). In the first step a conventional bulge test is conducted until a given pole height. In the second step the pre-bulged specimen is loaded with torsion coaxially to the rotational center of the specimen.

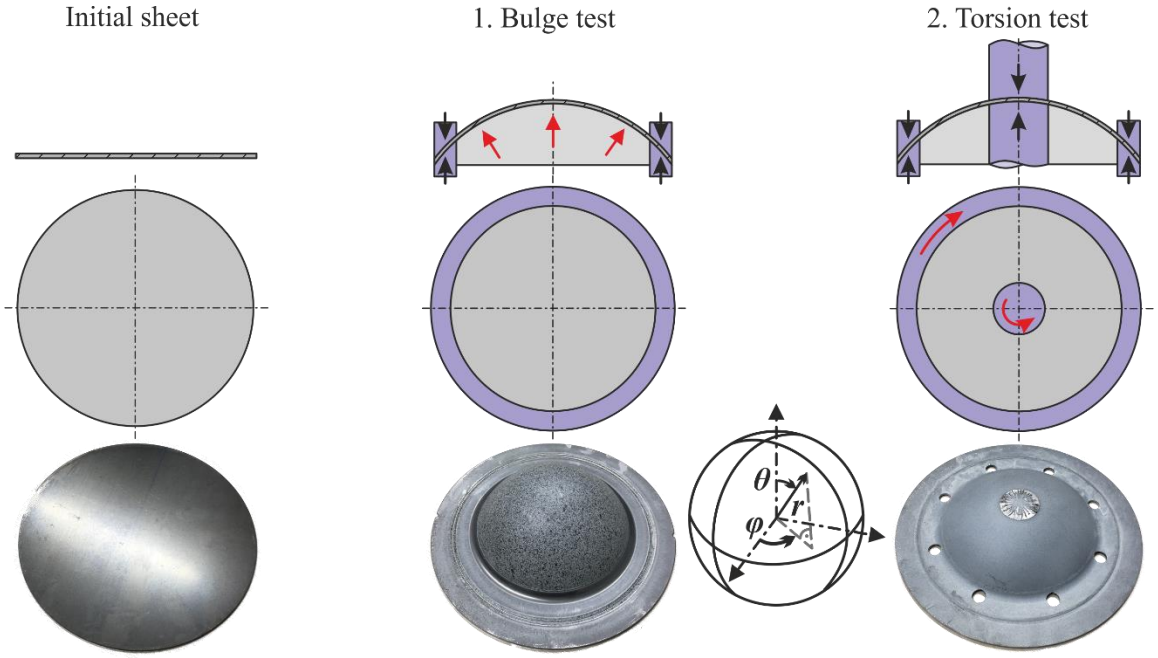

Figure 1. Scheme of proposed experiment.

For the analysis of the proposed experiment a spherical coordinate system e_r, e_θ, e_φ is used. Herein r is the radial distance from the center. For an ideal sphere the thickness of the sphere is parallel to e_r. The inclination, corresponding to meridian of the body is given by θ, while the azimuth in circumferential direction is given by φ.

During the hydraulic bulge test only σ_θ and σ_φ differ from zero. According to the Levy-Mises yield criterion the deviatoric part σ'_{ij} of σ_{ij} is directly proportional to the increment of plastic strain. Thus, the directions of the plastic strain increments are:

$$D_{\theta\theta} \neq 0;\ D_{\varphi\varphi} \neq 0;\ D_{rr} \neq 0 \tag{2.1}$$

In the subsequent step the semi-hemispherical sheet is loaded in torsion. Traphöner et al. [11] have evaluated the stress state for in-plane torsion of curved sheets and found that the shear stresses appear to be constant normal to the sheets surface. Thus, the only stresses differ from zero are $\tau_{\theta\varphi} = \tau_{\theta\varphi}$. The resulting directions of plastic strain increments are:

$$D_{\theta\varphi} = D_{\varphi\theta} \neq 0 \tag{2.2}$$

The scalar product of $D_{ij,\text{bulge}}$ and $D_{ij,\text{torsion}}$ will be zero. Hence, it is expected to achieve ideal orthogonal loading for characterization. At this point it is noteworthy to emphasize that the orthogonality of subsequent strains and not necessarily the orthogonality of the loading in the sense of stresses is relevant. E.g., loading of an isotropic sheet in rolling direction and subsequent in transverse direction would result in $\kappa = -0.5$.

2.1.2. Details of physical setup. The hydraulic bulge test is performed on a Zwick BUP1000 hydraulic testing machine in conjunction with a GOM Aramis digital imaging correlation (DIC) system. The correlation of sheet curvature radius to the applied pressure for a specific material can be calculated from an initial test. According to the realized pretest results, in the following the bulge test is stopped at a curvature radius of 65 mm. The inner die diameter is 120 mm.

For the subsequent in-plane torsions tests the setup for conventional in-plane torsion tests of plane sheets is used [12]. The setup is modified with adjusted inner clamps of a similar curvature according to the sheet shape. The lower clamp has a curvature radius of 65 mm, while the upper has been designed with a radius of 66 mm to consider the sheet thickness (Figure 2). Both clamps feature a diameter of 20 mm and grooves in radial direction to increase the applicable torque.

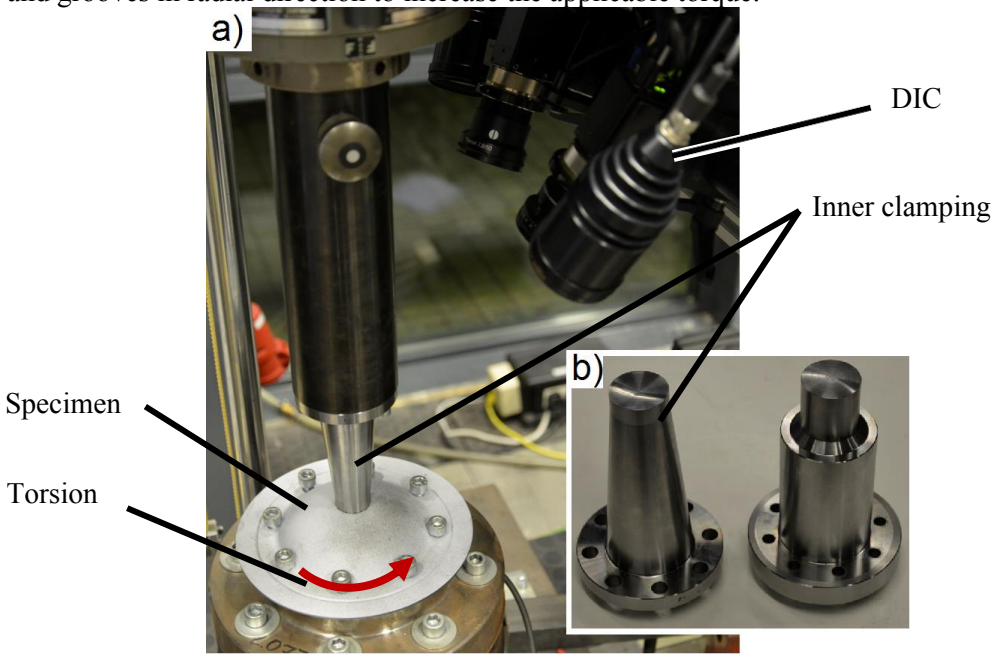

Figure 2. a) Setup for in-plane torsion of curved sheets, b) inner clamping (without grooves).

2.1.3. Material. DC04 is a low alloyed single-phase steel. Hence it is expected that dislocation glide is not restricted and the effect of strain-path change will be observable. For similar material DC06 the effect has already been reported [13].

2.2. Measurements

2.2.1. Strains. In both loading steps the deformation of the sheets is tracked via digital image correlation (DIC). Between the two test steps the sprayed DIC pattern is removed and re-applied. The strain gauge length are 1 mm for the bulge test and 0.35 mm for the torsion test, respectively. The bulge test is analysed at two positions. At first the centre point is recorded to obtain a stress-strain-curve, as required in [14]. Secondly, the final strain after unloading is measured in a distance of 10.6 mm from the centre. The equivalent von Mises strain is calculated for this point as $\bar{\varphi}_{bia} = \varphi_1 + \varphi_2 = 0.54$. This is the prestrain in the subsequent loading step. According to the measured strain the initial sheet thickness of 1.97 mm is reduced to 1.12 mm for subsequent torsion. In the case of the torsion test the local shear strain γ is calculated from the local maximum shear angle η_{max} as $\gamma = tan\,\eta_{max}$. The equivalent von Mises strain is then calculated as $\bar{\varphi}_{she} = \gamma/\sqrt{3}$. The authors are aware of the fact that different kinematic measures can be used for the analysis of shear tests (see e.g. [15]). For consistency with previous work [13], the current choices are made. The orientation of rolling direction has been tracked via permanent markers on the outer circumference. Both tests are evaluated at an angle of 45° with respect to the rolling direction, although no variation of strains under 0°, 45° and 90° is observed. The total equivalent strain in a bulge test with subsequent torsion is then given by $\bar{\varphi} = \bar{\varphi}_{bia} + \bar{\varphi}_{she}$.

2.2.2. Stresses. For the bulge test the biaxial stress is calculated according to DIN EN ISO 16808 [14]. In the subsequent torsion test findings of [11] are used to calculate the stress. They found the shear stresses to be constant in the normal of the sheet direction, for inclined sheets.

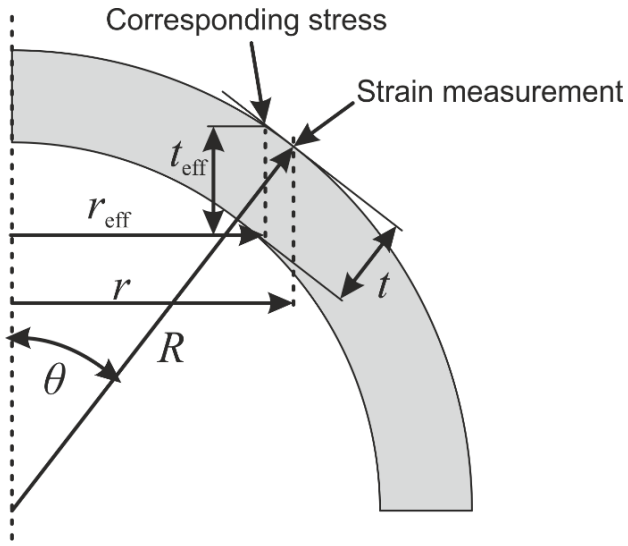

Figure 3. Calculation of effective radius.

Therefore the radius of the point where the strain is measured and the radius of the corresponding cross-section for stress evaluation are no longer identical in the torsion test. Figure 3 depicts the relevant geometric quantities. The shear stress $\tau_{\varphi r}$ depends on the effective radius r_{eff}

$$\tau_{\theta r} = \frac{M}{2 \cdot \pi \cdot r_{\text{eff}}^2 \cdot t_{\text{eff}}} \tag{2.3}$$

where *M* is the measured torque on the inner clamping, while the effective radius and the sheet thickness in z-direction are given as:

$$r_{\text{eff}} = r - \frac{1}{2} \cdot t \cdot \sin(\theta)\,; \;\; t_{\text{eff}} = \frac{t}{\cos(\theta)} \tag{2.4}$$

For $r = 10.6$ mm and $R = 65$ mm the corresponding angle $\theta = 9.39°$. The above equations have been validated for angles up to at least 35°.

2.3. Microstructure Analysis

To prove whether an orthogonal flow has been achieved and to analyze the deformation path dependent microstructure evolution in the tested specimen light microscopy (LM) and scanning-electron microscopy (SEM) are applied. The LM enables to get a macroscopic view of the form and orientation of the grains that have developed. Dislocation cells and sub-grain boundaries, responsible for hardening evolution are usually only visible in transmission-electron-microscope (TEM). Figure 4 shows the characteristic dislocation cell pattern for shear and tensile loading.

Due to a modern polishing procedure with polishing additive OPS and Vibromet device (Struers) it is possible to obtain sufficient contrast in the SEM to see sub-grain boundaries, which might also indicate change of deformation path.

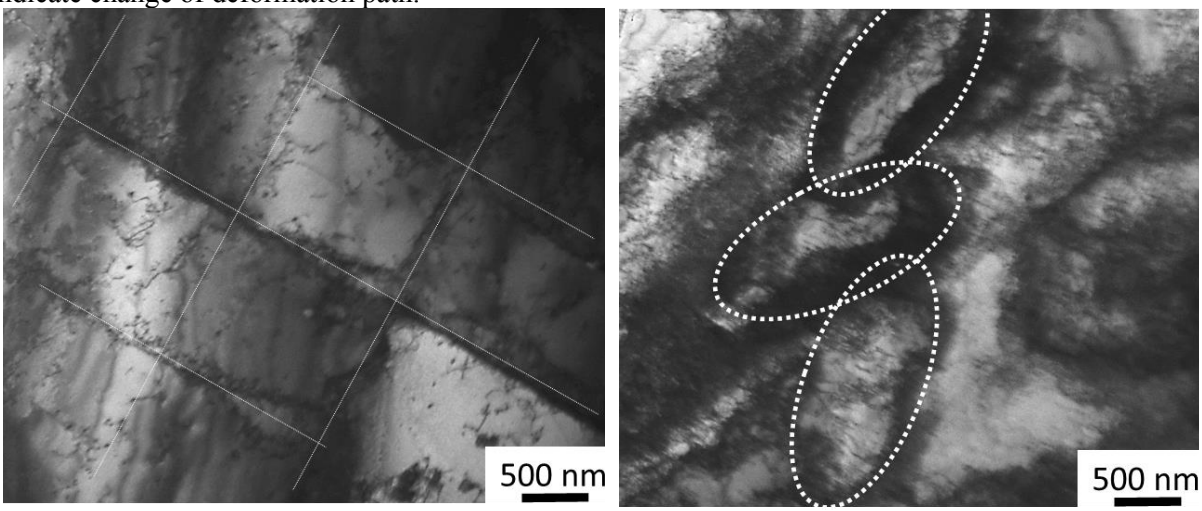

Figure 4. TEM images of DC04 after shear loading (left) and uniaxial tensile loading (right). Characteristic pattern of dislocation cells are highlighted.

3. Results and Discussion

3.1. Test curves

The resulting material response after orthogonal strain-path change (SPC) is depicted in Figure 5. For reference also the results for monotone shear loading are given. The SPC occurs at an equivalent strain of 0.54. The reloading yield stress is 477 MPa, while the monotonic torsion test yields a corresponding stress of 433 MPa. Therefore the instantaneous increase of yield stress is approximately 10%.

For continued torsion the hardening rate is reduced and the level of yield stress approaches the monotonic case. Thus both in the literature described effects of higher initial yield stress and (transient) decrease of hardening rate are observed.

Special attention must be paid to DIC measurements in shear tests. Due to the gradient of shear stress in radial direction the shear strains will develop with strongly varying intensity. This might result in an underestimation of the real shear strains [16]. For further support of these findings the microstructure is analyzed in the following.

3.2. Microstructure analysis

The microstructure analysis is performed on a specimen deformed with slightly modified pre-strain and tool set-up. The predecessor has lower pre-straining in bulge test and thus a worse fit to clamping (cf. Figure 6, bottom of Zone 1). A cross section cut along the radius of the specimen reveals that depending

on the radial position different mechanism with varying intensity were active (Figure 6). This result was expected due to the gradient of shear stress and shear strain with respect to the radius in the torsion test. Three different grain patterns can be identified. In Zone 3 the grains are stretched due to biaxial straining. In Zone 2 the authors assume that initially the same stretched grains were present, but have been divided by superposition of shear strains at thus a finer pattern is observable. In Zone 1 the grains feature no distinct pattern. The decreased grain size indicates severe compression deformation due to clamping. To achieve shear localization in a defined zone the manufacturing of a circumferential groove similar to an in-plane torsion test will be considered in future tests [11].

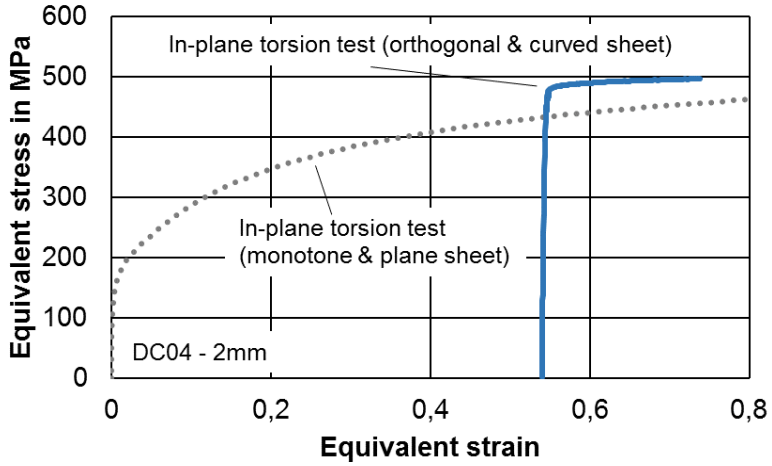

Figure 5. Stress strain diagram of the pre-bulged torsion experiment compared with monotonic torsion.

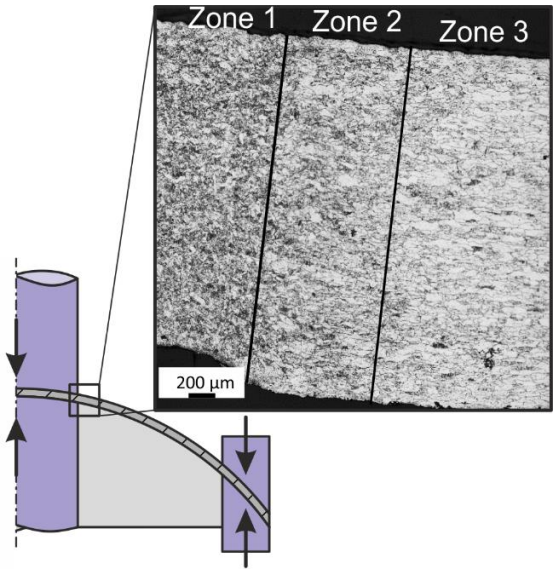

Figure 6. Micrograph of the etched cross section near inner clamping (LM).

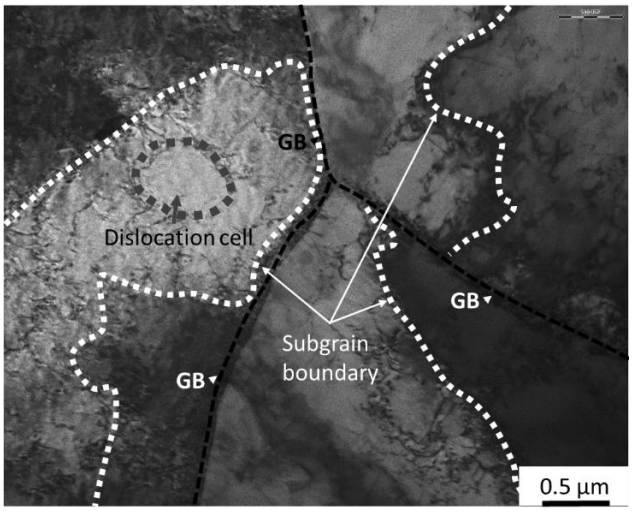

Figure 7. TEM image of sheet in the state of delivery. Relevant microstructure properties can be identified.

The TEM investigation of DC04 reveals dislocation cells and sub-grain boundaries on the micro-level, as well as grain boundaries (GB) on the meso-level (Figure 7), which are significant for plastic behavior and its evolution. Comparison of Scanning-electron-microscopy (SEM) images at different radial distances (Figure 8) supports the above findings. In a distance to the center the subgrains have a dimension of approximately 2 µm x 3 µm and the section is free from shear bands (SB). Close to the

inner clamping numerous shear bands have formed and the subgrain size reduced significantly by one order of magnitude. Both findings indicate high and localized strains characteristic of torsion.

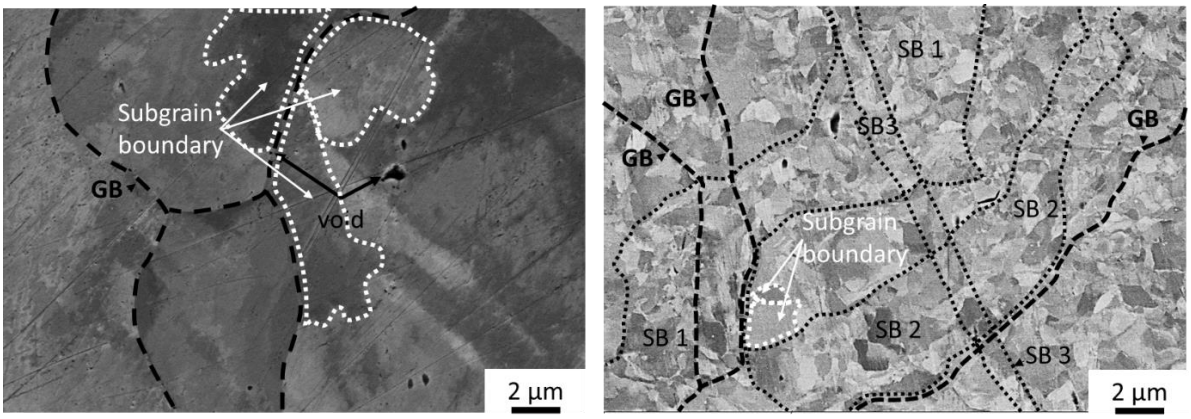

Figure 8. SEM image of the cross section at 90 mm distance from the centre (left) and 16 mm (right), respectively at the end of the test.

4. Conclusion

A novel experimental setup to characterize flow-induced anisotropy has been proposed. The orthogonality of the strain path has been demonstrated theoretically and is supported by micrographs of the evolving microstructure. Future tests should address the superposition of clamping strains and shear strains.

The macroscopic stress-strain curves show an increase of the initial yield stress after re-loading followed by a reduced hardening rate. The results are in agreement with the general observed effects for cross-hardening. The benefits of the proposed experiment are:

- High achievable pre-strains.
- No machining of subsequent specimen and thus avoidance of further residual stresses.
- Displacement field assessable over the entire process window.

The set-up requires a hydraulic test device, an in-plane torsion device and a DIC system. Additionally, the clamps of the existing equipment were modified.

Acknowledgement

The authors gratefully acknowledge funding by the German Research Foundation (DFG) within the scope of the Transregional Collaborative Research Centre on sheet-bulk metal forming (SFB/TR 73) in the project C4 ‘Analysis of load history dependent evolution of damage and microstructure for the numerical design of sheet-bulk metal forming processes’.

References

[1] Bauschinger J. Ueber die Veränderung der Elastizitätsgrenze und der Festigkeit des Eisens und Stahls durch Strecken und Quetschen, durch Erwärmen und Abkühlen und durch oftmal wiederholte Beanspruchung. München: K. Technischen Hochschule; 1886.

[2] Isik K, Wernicke S, Silva MB, Martins PAF, Tekkaya AE. Failure by fracture in sheet–bulk metal forming. *The Journal of Strain Analysis for Engineering Design*. 2016;**51**(5):387-94.

[3] Ghosh AK, Backofen WA. Strain-hardening and instability in biaxially stretched sheets. *Metallurgical Transactions*. 1973;**4**(4):1113-23.

[4] Rauch EF, Schmitt J-H. Dislocation substructures in mild steel deformed in simple shear. *Material Science and Engineering A*. 1989;**113**:441-8.

[5] Schmitt JH, Shen EL, Raphanel JL. A parameter for measuring the magnitude of a change of strain path: Validation and comparison with experiments on low carbon steel. *International Journal of Plasticity*. 1994;**10**(5):535-51.
[6] Schmitt JH, Fernandes JV, Gracio JJ, Vieira MF. Plastic behaviour of copper sheets during sequential tension tests. *Materials Science and Engineering: A*. 1991;**147**(2):143-54.
[7] Thuillier S, Rauch EF. Development of microbands in mild steel during cross loading. *Acta Metallurgica et Materialia*. 1994;**42**:1973-83.
[8] van Riel M, van den Boogaard AH. Stress-strain responses for continuous orthogonal strain path changes with increasing sharpness. *Scripta Materialia*. 2007;**57**(5):381-4.
[9] Noman M, Clausmeyer T, Barthel C, Svendsen B, Huétink J, van Riel M. Experimental characterization and modeling of the hardening behavior of the sheet steel LH800. *Materials Science and Engineering: A*. 2010;**527**(10-11):2515-26.
[10] Bouvier S, Gardey B, Haddadi H, Teodosiu C. Characterization of the strain-induced plastic anisotropy of rolled sheets by using sequences of simple shear and uniaxial tensile tests. *Journal of Materials Processing Technology*. 2006;**174**(1-3):115-26.
[11] Traphöner H, Clausmeyer T, Tekkaya AE. Material characterization for plane and curved sheets using the in-plane torsion test – an overview. *Journal of Materials Processing Technology*. 2018.
[12] Yin Q, Tekkaya AE, Traphoner H. Determining cyclic flow curves using the in-plane torsion test. *CIRP Ann-Manuf Technol*. 2015;**64**(1):261-4.
[13] Clausmeyer T, Gerstein G, Bargmann S, Svendsen B, van den Boogaard A, Zillmann B. Experimental characterization of microstructure development during loading path changes in bcc sheet steels. *Journal of Materials Science*. 2012;**48**(2):674--89.
[14] EN-ISO-16808. Determination of biaxial stress-strain curve by means of bulge test with optical measuring systems. Brüssel: CEN-CENELEC; 2014.
[15] Butcher C, Abedini A. Shear confusion: Identification of the appropriate equivalent strain in simple shear using the logarithmic strain measure. *International Journal of Mechanical Sciences*. 2017;**134**:273-83.
[16] Rahmaan T, Abedini A, Butcher C, Pathak N, Worswick MJ. Investigation into the shear stress, localization and fracture behaviour of DP600 and AA5182-O sheet metal alloys under elevated strain rates. *International Journal of Impact Engineering*. 2017;**108**:303-21.